Forcing of Ocean and Sea Ice Variability by the Southern Hemisphere Annular Mode

Alex Hall

University of California — Los Angeles

Department of Atmospheric Sciences

Box 951565

Los Angeles, CA 90095 USA

Martin Visbeck

Lamont-Doherty Earth Observatory

of Columbia University

PO Box 1000, 61 Route 9W

Palisades, NY 10964-8000

contact information:

Alex Hall

Tel: (310) 206-5253

e-mail: alexhall@atmos.ucla.edu

submitted to *Journal of Climate*

Abstract

Zonally-symmetric fluctuations of the mid-latitude westerly winds characterize the primary mode of atmospheric variability in the southern hemisphere during all seasons. This is true not only in observations, but also in an unforced 15,000 yr integration of a coarse resolution (R15) coupled ocean-atmosphere model. Here we document how this mode of atmospheric variability, known as the Southern Annular Mode (SAM), generates ocean circulation and sea ice variations in the model integration on interannual to centennial time scales that are tightly in phase with the SAM. The positive phase of the SAM is associated with an intensification of the surface westerlies over the circumpolar ocean (around 60°S), and a weakening of the surface westerlies further north. This induces Ekman drift to the north at all longitudes of the circumpolar ocean, and Ekman drift to the south at around 30°S. Through mass continuity, the Ekman drift generates anomalous upwelling along the margins of the Antarctic continent, and downwelling around 45°S. The anomalous flow diverging from the Antarctic continent also increases the vertical tilt of the isopycnals in the Southern Ocean, so that a more intense circumpolar current is also closely associated with positive SAM. In addition, the anomalous divergent flow advects sea ice further north, resulting in an increase in sea ice coverage. Finally, positive SAM drives increases in poleward heat transport at about 30°S, while decreases occur in the circumpolar region. Ocean and sea ice anomalies of the opposite sign occur when the SAM is negative. The ocean and sea ice fluctuations associated with the SAM constitute a significant fraction of simulated ocean variability poleward of 30°S all year round. The robustness of the mechanisms relating the SAM to oceanic variability suggests that the SAM is likely an important source of large-scale variability in the real southern hemisphere ocean.

1 The atmospheric jet stream and southern hemisphere geography

If the earth's surface were perfectly uniform, the temperature response to the zonally-symmetric equator-to-pole gradient in solar forcing would also be zonally-symmetric. This would generate, in turn, a mid-latitude jet stream with zonally-symmetric statistics of variability. Of course, the earth's surface is not uniform. In the northern hemisphere (NH), there are large zonal contrasts in surface type. In crude terms, there are two north-south oriented strips of ocean interrupted by two strips of land. These zonal asymmetries set up the well-known wavenumber 2 stationary wave pattern in the climatological mean state of the NH jet stream. (Broccoli and Manabe (1992), by comparing atmospheric simulations with and without mountains, provide evidence that orography is the main reason for these stationary undulations of the NH jet stream.) Because of the wavenumber 2 pattern, the most baroclinically unstable parts of the jet stream are concentrated over the North Atlantic and Pacific, giving rise to the NH Atlantic and Pacific storm tracks.

Just as the zonal contrasts in NH geography disrupt the zonal symmetry in the NH jet stream, the relative zonal uniformity of southern hemisphere (SH) geography reinforces the zonal symmetry of the SH mid-latitude atmospheric jet stream: Directly over the SH pole sits a permanently frozen continent topped with a glacier a few kilometers thick. This continent is surrounded by an ocean extending more than halfway to the equator. Relatively small land masses interrupt the zonal symmetry further north, but the surface area all the way to the equator is overwhelmingly dominated by ocean. The large thermal contrast between the polar continent and the tropical ocean generates an intense jet stream which is much more zonally-symmetric than its NH counterpart.

Just as the jet stream is the dominant feature of the mid-latitude atmospheric circulation, it also dominates the signatures of variability. For example, if one examines the mode of atmospheric pressure variability that accounts for the most variance using techniques such as EOF

analysis, one sees a clear out-of-phase relationship between pressure over the pole and pressure in mid-latitudes. The ring-like character of this pattern has given rise to the term 'annular mode' to refer to the vacillations of the jet stream in both hemispheres (see Thompson and Wallace (2000)). The concept of an annular mode also derives from an idealized picture of an atmosphere overlying a completely uniform surface. In atmospheric models with no orography or land-sea contrast, the oscillation of mass associated with jet stream variability is perfectly zonally-symmetric and ring-like (James and James (1992), Yu and Hartmann (1993), Lee and Feldstein (1996), Robinson (1996)).

All evidence indicates that these turbulent fluctuations of the jet stream can be generated entirely by the atmosphere. For example, using an atmosphere-only general circulation model with seasonally-varying sea surface temperatures, Hartmann and Limpasuvan (2000) obtain annular modes in both hemispheres that are nearly identical to observations. Furthermore, numerous researchers (DeWeaver and Nigam (2000a), DeWeaver and Nigam (2000b), Limpasuvan and Hartmann (2000), Limpasuvan and Hartmann (1999), Hartmann and Lo (1998)) have diagnosed the internal atmospheric dynamics responsible for the annular mode: Both hemispheres' jet streams are substantially modified by the synoptic-scale eddies they spawn, giving rise to mutually-reinforcing feedbacks between eddies and the mean flow. An anomaly in the jet stream generates anomalous eddy activity of the same sign, which in turn strengthens the jet stream anomaly through eddy momentum fluxes. The vacillations of the jet stream are then largest where eddy activity is largest. Because of the zonal asymmetries of NH geography, eddy activity and consequently jet stream variability is largest in the Atlantic and Pacific storm track regions. So the anti-correlation between mid and high latitude atmospheric pressure that is the hallmark of the annular mode is strongest in the Atlantic and Pacific sectors. In the SH, because of its relative zonal symmetry, eddy activity is much more evenly distributed among all longitudes. This, in

turn, gives rise to an annular mode that is much more zonally symmetric than its NH counterpart (Thompson and Wallace (2000)). That eddy-mean flow interactions are key to understanding the annular mode is also suggested by the fact that the annular modes in both hemispheres exhibit little variability on time scales shorter than the synoptic eddy time scale. For example, Hartmann and Lo (1998) show that the e-folding time scale of the auto-correlation of the observed southern hemisphere annular mode (SAM) index is approximately 10 days.

The SAM is different from its NH counterpart (NAM) not only in its much higher degree of zonal symmetry, but also in its relatively weak seasonal variability, which reflects the relatively weak seasonality of the equator-to-pole temperature gradient and atmospheric jet stream. Hartmann and Lo (1998) found that the SAM weakens somewhat in the summertime but retains its structure in both observations and an atmospheric model simulation. This is in contrast to the NAM, which practically disappears in summertime.

In this study, we focus not on the internal atmospheric dynamics of the SAM, but on the implications of a highly zonally-symmetric and year-round mode of atmospheric variability for the rest of the SH climate system, in particular sea ice and the ocean. While the relatively high degree of zonal symmetry of SH geography reinforces the zonally-symmetric character of the primary mode of internal atmospheric variability (i.e. the annular mode), it also facilitates hemispheric-scale synchronization of ocean variability with annular mode forcing. Even if by some improbable mechanism the NAM were perfectly zonally symmetric in spite of the zonal asymmetries of NH geography, the response of the NH oceans to this forcing could never be zonally symmetric or coherent between ocean basins, both because of the huge differences in geometry between the ocean basins and their physical separation. In the SH, on the other hand, very little land exists at the latitudes where annular mode variability is strongest. This, coupled with the relative zonal symmetry of the annular mode forcing itself, sets up very favorable conditions for atmosphere-

ocean co-variability: when the SAM is in its positive phase, surface westerlies strengthen at all longitudes of the circumpolar ocean, and the ocean has to respond in a similar way at all longitudes, creating a coherent, zonally-symmetric ocean mode of variability tightly in phase with the SH annular mode. In this study, we show that much of the variability throughout the entire SH ocean poleward of 30°S in a coupled ocean-atmosphere model simulation can be linked directly to the SAM.

These results lead us to a new perspective on internal climate variability in the mid to high latitudes of the SH. Adopting the view of a synchonously-varying, zonally-symmetric system from the top of the atmosphere down to the ocean bottom is useful because it probably captures a good deal of the variability in this region. Of course, this hypothesis must be tested against the observational record to be fully validated. However, the simulated SAM is realistic enough and the mechanisms we identify relating the SAM to ocean variability are robust enough that it seems likely the observed record will reveal similar results to this simulation. Few hypotheses for what causes SH climate variability have been proposed. In fact the mid to high latitudes of the SH remains a critical blind spot in our understanding of the global climate system from both theoretical and observational perspectives. The ideas presented in this paper therefore constitute a significant, though preliminary, step forward.

We begin by describing the coupled model simulation (section 2) and the annular modes it produces (section 3). Then in section 4, we describe and document the mechanism that links the SAM to SH ocean circulation variability, followed by a description of its associated impacts on other features of the ocean, such as heat transport, SST, and sea ice (section 5). Finally, we discuss the possible implications of these results for SH climate in section 7.

2 Model Description

To study the role of the SAM in SH sea ice and ocean variability on interannual to centennial time scales, we examine the variability in the middle 5,000 yrs of a 15,000 yr integration of a coupled ocean-atmosphere model. What follows is a brief description of this model. It is described in greater detail in Manabe et al. (1991). The model has a global domain with geography as realistic as possible given its computational resolution (see the depictions of model geography in fig 1). The atmospheric component has nine vertical levels, with horizontal distributions of atmospheric variables represented by spherical harmonics and grid-point values with 4.5° latitude by 7.5° longitude spacing (Gordon and Stern, 1982). Sunshine varies seasonally, but not daily. Cloud cover is predicted based on relative humidity. A land surface model computes surface fluxes of heat and water. Continental ice sheets are prescribed. The ocean component (Bryan and Lewis, 1979) employs a full finite-difference technique and has a regular grid system with approximately 4.5° latitude by 3.8° longitude spacing. There are 12 vertical levels in the ocean. The effects of mesoscale eddies are represented by diffusion of potential temperature and salinity on constant density surfaces. The model also has some diapycnal diffusion for numerical stability. A sea ice model is also included (Bryan, 1969). It computes sea ice thickness based on thermodynamic heat balance. Advection of ice by ocean currents is also included, so long as the ice thickness is less than 4m. When the ice thickness if greater than 4m, divergent ice flow with surface currents is allowed, but convergent flow is not. This is meant to mimick the inability of ocean currents to transport sea ice into regions where the ice pack is already very thick. The atmospheric and oceanic components exchange heat, water, and momentum once a day.

The coupled model's quasi-equilibrium initial condition is obtained by separate integrations of the atmospheric and oceanic components using observed surface boundary conditions (sea surface temperature (SST), sea surface salinity (SSS) and sea ice thickness). When the inte-

gration of the coupled model begins from this initial condition, the simulated climate drifts toward a less realistic equilibrium state. To reduce drift, the fluxes of heat and water at the ocean-atmosphere interface are adjusted by given amounts before they are imposed on the ocean surface. The flux adjustments are determined prior to the coupled model run from separate integrations of the atmosphere and ocean models. They do not change from one year to the next and are independent of the SST and SSS anomalies that develop during the simulation. Thus they neither damp nor amplify these anomalies in any systematic way. Although the adjustments do not eliminate the shortcomings of the model (Marotzke and Stone, 1995), they do help prevent rapid drift from the initial state. Such drift can seriously distort the internal climate variability that is the subject of this study.

Although this model's resolution is coarse, and its parameterizations are not complicated, it is very computationally efficient, allowing for very long integrations, such as the 15,000 yr run we analyze in this paper. This is the longest coupled model experiment in existence as of the writing of this paper, and its extraordinary length has two advantages. First, it allows for analysis of very low-frequency climate variability. See, for example, the results for centennial and longer time scales presented in fig 7. Second, it makes for extraordinarily trustworthy statistics. For example, in this study, we analyze 5,000 yrs of data. Suppose one examines the correlation between 5000-yr-long, annual-mean time series of two different model variables. For all correlations greater in magnitude than 0.03, the probability that no relationship exists between the two time series would be less than 1%. So the 99% 'significance level' for such a long time series is essentially zero.

3 Simulation of Annular Modes

To assess the realism of the model's simulation of annular modes, we examined the leading mode of the model's surface pressure field in both hemispheres. In keeping with convention,

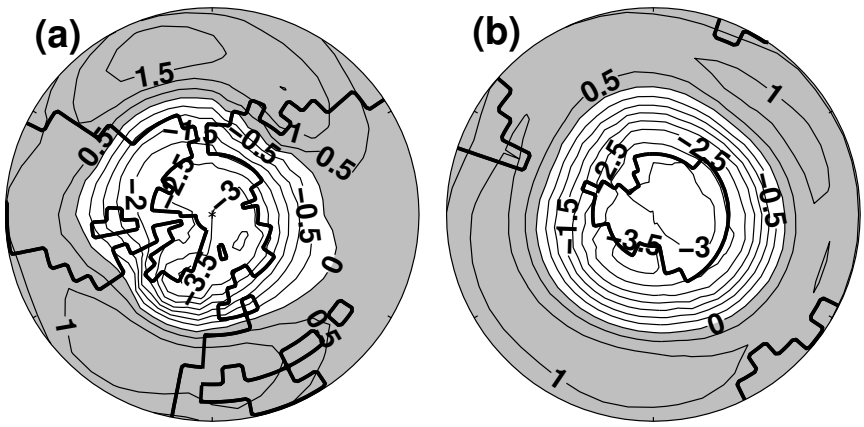

Figure 1: (a) The pattern associated with the first EOF of variability for NH DJF seasonal mean surface pressure data poleward of 9°N. This pattern accounts for 24% of the variance. (b) as in (a), except for SH JJA seasonal mean surface pressure data poleward of 9°S. This pattern accounts for 34% of the variance. The surface pressure fields were area-weighted prior to the computation of the EOFs. Positive areas are grey, while negative areas are white. This convention is observed in all subsequent figures. Units are hPa.

we restricted our analysis to wintertime, when the jet stream and storm tracks are at their peak. In the NH (fig 1a), the leading mode is characterized by an out-of-phase relationship between surface pressure over the Arctic and surface pressure in the North Atlantic and Pacific, as is the case with the observed leading mode (see fig 3d of Thompson and Wallace (2000)). In the North Atlantic sector, the NAM resembles the observed closely, with the nodes of the simulated and observed patterns both located at about 55°N. In the North Pacific sector, the simulated and observed are less similar in that the node of the simulated pattern lies at about 55°N, while the node in the observed pattern lies further north, at about 60°N. In addition, the North Pacific lobe of the model's pattern is more pronounced than the Atlantic lobe. The opposite is true in observations.

In the SH (fig 1b), a clear out-of-phase relationship between surface pressure in mid and high latitudes is also apparent. Like the observed (see fig 3c of Thompson and Wallace (2000)), the SH pattern is much more zonally-symmetric than in its NH counterpart and its node lies directly over the center of the circumpolar ocean at about 55°S. In both the NH and SH, the model's annular mode is similar to the observed. In spite of its coarse computational resolution, the model can resolve the eddies whose interaction with the mean flow generates the annular modes. This is consistent with the findings of Manabe and Hahn (1981). Analyzing a simulation employing only the atmospheric component of this model, they found that it approximately reproduces the observed magnitude of daily, monthly, and annual-mean surface pressure variability in mid to high latitudes. This indicates the atmospheric model has a realistic amount of eddy activity.

In section 1, we noted that while the NAM practically disappears during summertime, the SAM remains the dominant feature of variability throughout the year in both observations and an atmospheric model similar in structure to the model we analyze but with double the resolution (Limpasuvan and Hartmann (2000)). Examining the dominant mode of pressure variability for

all four seasons (fig 2), it is clear that this coarse resolution model exhibits the same behavior. The pattern is very ring-like all year round, with the positive phase associated with a low over the pole, and a high in mid-latitudes. The intensity of the modes increases slightly during the cold months, consistent with the slight intensification of the equator-to-pole temperature gradient.

Because of the relatively weak seasonality of the simulated SAM, we will examine its role in forcing ocean variability from an annual-mean perspective. We constructed a time series of the dominant mode of annual-mean pressure variability by performing EOF analysis on annual-mean surface pressure data. We will be correlating and regressing annual-mean ocean variables with this time series to illuminate the relationships between the SAM and ocean variability. Not surprisingly, the pattern associated with this time series (not shown) very closely resembles the patterns seen in fig 2. It also accounts for a similar amount of the total variance: 39%. This is a large fraction of the variability, especially in view of the fact that the domain included in the EOF analysis extends to 9°S, where a significant proportion of surface pressure variability is unlikely to be directly related to the variability of the mid-latitude jet stream. A comparable amount of variability (about 30%) is attributable to the SAM in the real climate (David Thompson, personal communication).

Because of the strong zonal symmetry of the SAM throughout the year, taking a zonal-mean perspective can provide a concise means of conveying information about its behavior. To provide a brief overview of the behavior of the SAM in the model atmosphere, we show the vertical structure of zonal-mean zonal, meridional, and vertical velocity anomalies associated with the positive phase of the SAM throughout the atmosphere (fig 3). From about 45°S to 75°S, positive SAM implies intensification of the westerly winds (panels a and b) throughout the model atmosphere. From 45°S to 20°S, on the other hand, easterly anomalies occur when the SAM is positive. This is consistent with a poleward shift of the atmospheric jet stream. This is also the

pattern seen in observations (see fig 3a of Thompson and Wallace (2000)). Anomalies in the meridional winds are also seen (panels c and d). The main features are poleward flow due to friction from the westerly anomaly from 45°S to 75°S, and equatorward frictional flow stemming from the easterly anomaly from 45°S to 20°S. Panels e and f demonstrate that positive SAM is associated with subsidence throughout the mid and lower atmosphere from 55°S to 35°S, and rising motion throughout the mid and lower atmosphere from 55°S to 80°S. This is likely due to the divergent meridional flow at the surface around 45°S, and the convergent meridional flow near the pole. In addition, the poleward movement of the jet stream and associated eddy activity may enhance rising motion north of 55°S and reduce it south of that point.

4 Co-variability in the Atmosphere and Ocean

In the previous section, we discussed how much of the variability of the simulated and real atmosphere in the mid to high latitudes of the SH is attributable to the SAM. In this section, we examine the extent to which ocean variability can be related to the SAM. As outlined in section 1, there are reasons to expect co-variability between the SAM and the ocean circulation.

To understand how the SAM affects SH ocean variability, we must first understand how the atmosphere influences the mean state of the SH ocean. The high degree of zonal symmetry of SH geography is largely responsible for the peculiar state of the ocean in this region (Gill and Bryan (1971)). In the real and simulated worlds, surface westerly winds prevail in much of the circumpolar ocean region (fig 4a). This drives Ekman drift to the north at all longitudes, creating divergent surface flow away from the Antarctic continent. This divergent flow prevents warm waters from reaching the circumpolar region, accentuating the isolation of the Antarctic continent. The inability of warm water to penetrate to higher latitudes in the SH sets up an extremely sharp density gradient between the waters near the Antarctic continent and the waters

north of the Drake Passage. This density gradient, in turn, drives the intense eastward circumpolar current. The simulated surface manifestation of this current is shown in fig 5a. The relative zonal asymmetry of NH geography makes for a vivid contrast between the ocean circulations of the two hemispheres: in the NH, the presence of north-south oriented continental margins in mid-latitudes where surface westerlies dominate results in the development of western boundary currents rather than a circumpolar current.

Since fluctuations of the surface westerlies are a feature of the SAM, and since these same surface westerlies are responsible for the large-scale features of the SH ocean circulation (i.e. divergence away from the Antarctic continent and the circumpolar current), it makes intuitive sense that the SAM would generate variability in these features of the ocean circulation. At the surface, positive SAM manifests itself as a poleward migration of the mean westerly winds. A one sigma positive SAM anomaly implies an order 10% intensification of the westerly wind stress in the circumpolar ocean region, and a weakening of the westerly wind stress further north (fig 4b). As suggested by fig 4c, these anomalies account for a very large amount of the overall wind stress variability; In most portions of the circumpolar ocean, the correlation between the SAM index and the zonal wind stress exceeds 0.6. Further north, the anti-correlation between the zonal wind stress and the SAM is also large, dipping below -0.4 in many areas.

How then do these wind stress anomalies affect the ocean circulation? In the circumpolar region, where positive SAM implies intensification of the westerly winds, flow mainly to the north occurs (fig 5b). Further north, where westerlies weaken, southward flow results. These current anomalies are very similar to those that would result if the wind stress pattern associated with positive SAM resulted only in Ekman drift in the 50m-deep first layer of the model ocean (fig 5d). This indicates that the current anomalies of fig 5b can be directly related to the wind stress through the Ekman mechanism. There are however, hints of disagreement between figs 5b

and d. For example, in the circumpolar region, the current anomalies of fig 5b are generally tilted slightly more to the east. As we discuss below, this can be related to intensification of the circumpolar current. Examination of the correlation between meridional ocean currents and the SAM index (fig 5c) reveals that the current anomalies of fig 5b represent a very significant fraction of surface current variability. The correlations in the circumpolar ocean exceed 0.6 in many regions.

We have shown that the SAM has a very direct and significant effect on simulated surface current variability in the southern ocean. What about the rest of the southern ocean, which is not in such close contact with the atmosphere? The zonal symmetry of the surface current response to the SAM indicates that information about ocean response to the SAM is not lost by taking a zonal-mean perspective. Fig 6 summarizes the relationship between the zonal-mean meridional and vertical ocean flow throughout the southern hemisphere. Consistent with figs 5b and c, figs 6a and c show that the SAM is very significantly correlated with northward surface flow between 45 and 70°S, and southward surface flow from about 20 to 40°S. This results in convergence and downwelling near 45°S, and divergence and upwelling near the Antarctic continent at about 60°S (figs 6b and c). The vertical motion penetrates nearly to the bottom of the ocean and is highly correlated with the SAM index to depths of two to three thousand meters.

Return flow at depth must balance the surface meridional flow anomalies. If the model ocean bottom were flat, one would expect the return flow to be confined to a turbulent frictional layer at the ocean bottom. Because of the model's coarse resolution, its bottom topography is relatively smooth, varying between 3000-4500 m over most of the circumpolar region. Accordingly, the simulated return flow (most evident in the fig 6a) resembles what would be expected from a flat bottom ocean. With higher resolution and more realistic bottom topography, the surface meridional flow anomalies would very likely still occur. However, rather than being confined

to a turbulent frictional layer at the bottom, significant return flow at depth could be supported geostrophically through zonal pressure differences across topography. This return flow would reflect the complexity of the real ocean's bottom relief, and would perhaps be more evenly distributed throughout the ocean. This implies that the pattern of fig 6a would likely change with resolution, though it also suggests that a significant portion of variability of the deep ocean circulation in this region would be related to the SAM no matter what the model resolution.

Much of the variability in the strength of the circumpolar current ought to be traceable to the SAM as well. As discussed above, the existence of the circumpolar current can be traced partly to the fact that westerly winds generate divergent flow away from the Antarctic continent. So it seems intuitive that the variations in the surface westerlies ought to produce variability in the circumpolar current. Fig 7 confirms this in the simulation. The bottom panel shows the coherence between the SAM and the circumpolar current. On time scales between 2 and 25 years, a very significant coherence between the SAM and the circumpolar current is observed. The coherence drops off to very low values on time scales between 25 and 150 yrs.

Though a detailed analysis of the time-scale-dependence of the coherence between the SAM and the circumpolar current strength is beyond the scope of this paper, preliminary analysis indicates that the dropoff in coherence on the 25-150 yr time scale can be explained the presence of another mode of variability—most likely internal to the ocean—that is most active on these time scales. This is made clearer by an examination of the spectra of the circumpolar current and the SAM index (fig 7a). On time scales from 2 to 500 yrs, the SAM index spectrum is rather white, while the circumpolar current spectrum is very red, with a pronounced hump on time scales of 25 to 150 yrs. The lack of a similar spectral peak in the SAM index, coupled with the lack of coherence between the SAM and the circumpolar current on the 25-150 yr time scale, strongly indicates that another mode of variability exerts primary control on the circumpolar

current on these time scales. It should be emphasized that no similar time-scale-dependence of the relationship between the SAM and meridional and vertical currents is seen (i.e. the statistics presented in figs 5 and 6 are practically the same for all resolvable time scales.)

5 Impact on heat transport, SST, and sea ice

The strong zonally-symmetric projection of meridional ocean current variability onto the SAM (figs 5 and 6) suggests the SAM might also have a significant influence on meridional ocean heat transport. To test this, zonal-mean ocean heat transport was calculated at all latitudes of the SH (fig 8a). The model ocean transports heat poleward throughout the SH, with the amount decreasing from a peak of about one petawatt at 15°S to zero at 80°S. Available observations indicate that the real ocean transports a comparable amount of heat (fig 8a). The correlation and regression coefficients between the SAM index and the ocean heat transport show particularly significant relationships at about 50°S, where a reduction in poleward ocean heat transport is associated with positive SAM, and 30°S, where positive SAM is associated with an increase in poleward heat transport. These anomalies are approximately a tenth as large as the mean heat transport, and are consistent in sign and meridional extent with the surface current anomalies excited by the SAM: During positive SAM, Ekman drift transports cold water northward in the southern ocean, thereby reducing poleward heat transport. Likewise, Ekman drift to the south around 30°S enhances it.

The heat transport anomalies associated with positive SAM result in a divergence of heat centered at about 55°S, and a convergence of heat centered at about 40°S. Since the heat transport anomalies are focused at the surface, this convergence and divergence of heat manifests itself in SST anomalies. The SST anomalies account for a fair amount of the variability in zonal-mean SST (fig 9a). Fig 9b demonstrates that for a 1 sigma SAM anomaly, zonal-mean SST

decreases in the circumpolar region by about 0.1°C, while it increases by about 0.05°C in the subtropics. These anomalies are fairly small probably because the SST gradients are not large in this region, limiting the effect of the current anomalies associated with the SAM on SST. This is not inconsistent with the relatively large impact of the SAM on meridional heat transport since the effect on SST, small though it is, is the same sign at nearly all longitudes.

SST is obviously an important climatic variable. Sea ice is also critical because of its high albedo relative to the open ocean and its role as a thermodynamic buffer between the atmosphere and the ocean. A portion of the current anomaly pattern associated with the SAM (fig 5b) lies within the ice-covered regions of the southern ocean (fig 10a). To the extent that the simulated sea ice distribution is affected by surface currents, one might expect the SAM to force sea ice variability through its forcing of surface currents. The correlation between the SAM index using surface pressure data from the months of June through November only (JJASON) and ice thickness during these same months demonstrates this (fig 10b). (The JJASON period was chosen because ice extent in the SH is greatest during this half of the year. When sea ice reaches its seasonal minimum during late SH summer and early fall months, ice extent is reduced nearly to the margins of the Antarctic continent in both model and observations, and is barely affected by the open-ocean Ekman drift anomalies forced by the SAM.) As ice is advected northward during positive SAM, ice thickness decreases near the coast of Antarctica and increases further north. The correlations with the SAM are modest in most places, with the possible exception of the South Indian basin, where correlations reach values as high as 0.4. Since the current anomalies are so well correlated with the SAM (fig 5c), this indicates that local sea ice thickness is mostly determined not by current anomalies, but by local thermodynamic processes.

It is possible that the sea ice pattern associated with the SAM occurs because sea ice anomalies are generating SAM variability. However, this seems unlikely, because the sea ice

pattern of fig 10b is so obviously related to the ocean current anomaly pattern of fig 5b, which itself is almost certainly forced by the SAM.

While the correlation pattern shown in fig 10 shows that the SAM has only a modest impact on local ice thickness variability, the high degree of zonal symmetry in the pattern suggests that the impact on total areal ice coverage might be more significant. To examine this issue, we created an ice coverage time series, defining the ice margin as the location where ice thickness falls below 50cm. The correlation between the JJASON SAM index and this time series is 0.51, implying that the SAM accounts for a large share of the simulated variability in total sea ice coverage. The regression of the ice coverage time series onto the SAM index is 5.9 X 10^5 km^2, as compared to a total mean ice coverage of 167.4 X 10^5 km^2. Even a relatively weak one sigma anomaly in the SAM is associated with a significant increase in sea ice coverage.

A study of the observed relationship between sea ice and the SAM is beyond the scope of this paper. Such a study would be difficult as continuous multi-year time series of sea ice and surface pressure observations in the SH poleward of 45°S are still somewhat sparse, though recent satellite observation of sea ice has improved the observational record. However, statistically significant relationships between NH sea ice and the NAM have been documented using the much better meteorological and oceanographic time series of the NH (Kwok and Rothrok 1999, Kwok 2000). Given this observational evidence from the NH and the modeling evidence presented in this paper, it seems likely that statistically significant relationships between SH sea ice and the SAM will eventually also be found in the observations.

Because of the high albedo of sea ice compared to the open ocean, we also examined the possibility that the SAM influences the total radiative budget of the atmosphere through its effect on sea ice coverage. Fig 11a confirms that zonal-mean net incoming shortwave radiation (ISR) is reduced by about 1 W/m^2 around the latitude of the sea ice margin for a 1 sigma positive

anomaly in the SAM. Fig 11b shows how this anomaly compares to the SAM's effect on the other element of the earth's radiative budget–outgoing longwave radiation (OLR). The SAM is associated with a 0.5 W/m^2 increase in the OLR at about 40°S, and an decrease of about the same amount poleward of 60°S. The OLR increase at 40°S can be accounted for by a decrease in clouds (fig 11d). The clouds decrease at this latitude because of a poleward migration of the jet stream, and a likely reduction in baroclinic activity and rising motion in consequence (fig 3f). The increase in ISR at 40°S is also attributable to this loss of cloud. The changes in ISR and OLR almost counterbalance one another in the net radiative budget at 40°S (fig 11c), so that the dominant feature of the SAM impact on zonal-mean net radiation is a decrease in net radiation at 60°S, which results from the expansion of sea ice coverage.

6 Summary

To summarize our findings, we created a schematic drawing of the changes in the atmosphere and ocean that occur in when the SAM rises 1.5 standard deviations higher than its mean value (fig 12). As a companion to fig 12, we provide a table showing the magnitude of the changes depicted in the drawing, as well as the correlation between these variables and the SAM index (table 1). For reference, the mean values of the variables are also given in table 1.

In the atmosphere, positive SAM is associated a poleward movement and intensification of the atmospheric jet stream. This results in an intensification of the westerlies at about 55°S and a weakening at about 35°S. Frictional meridional flow at the surface is generated by the zonal wind fluctuations. Based on the correlation coefficients in table 1, rows (a)-(d), the SAM accounts for nearly all the variability in zonal-mean surface winds at these locations. In magnitude, the anomalies are about 20% of their mean values. The surface meridional flow anomalies result in divergence around 40°S, and convergence at around 65°S. To satisfy mass continuity, subsi-

dence occurs around 40°S, while rising motion occurs at around 65°S. This vertical motion may also be the signature of the poleward migration of baroclinic eddy activity due to the poleward movement of the jet stream.

The ocean receives information about the state of the SH atmosphere's annular mode mainly through frictional transfer of momentum at the air-sea interface. The surface westerly anomalies associated with positive SAM excite northward Ekman flow from about 45 to 65°S, while the surface easterly anomalies generate southward Ekman drift from 30 to 45°S. These surface current anomalies are one to two-thirds as large as their mean value. To satisfy mass continuity, a 40% increase in upwelling occurs around the Antarctic coast, while a 15% decrease in upwelling takes place at about 45°S. The anomalous flow diverging from the Antarctic continent also increases the vertical tilt of the isopycnals in the Southern Ocean, so that a more intense circumpolar current is also associated with positive SAM: A 1.5 sigma SAM anomaly increases the simulated transport through the Drake Passage by about 1 Sverdrup. In addition, the anomalous divergent flow advects sea ice further north, resulting in an about a 5% increase in sea ice coverage. Meridional heat transport is also affected: order 15% increases in poleward heat transport occur at about 30°S, while order 20% decreases occur in the circumpolar region. The anomalies in meridional heat transport create heat convergence at about 40°S and heat divergence at about 55°S. This generates modest SST anomalies at these locations. As the correlations listed in the final column of table 1 indicate, a major fraction of large-scale zonal-mean ocean variability poleward of 30°S can be related to the SAM. The variability in ocean circulation is particularly coherent with the SAM.

7 The potential role of the SAM in climate

To evaluate the significance of these results, one must first assess the realism of the model. Its coarse resolution is potentially its most serious shortcoming. However, as noted in section 3, the resolution of the model atmosphere is high enough to simulate a SAM very similar to its observed counterpart, both in its spatial structure and its share of overall atmospheric variability. For the purposes of this study, the atmospheric model therefore does a reasonable job of providing the ocean with realistic forcing, in spite of its coarse resolution. In the ocean, the most obvious implication of the model's coarse resolution is that it cannot simulate mesoscale eddies. Since these eddies interact in significant ways with the circumpolar current, the circumpolar current is probably not realistic in structure or strength. In fact, the simulated mean strength of the circumpolar current (76 Sv) is less than observed estimates. For example, Baker (1982) estimates that the strength of the real circumpolar current is 113 Sv. In addition, the actual Southern Ocean is a site of convection and deep water formation, a process which probably occurs on spatial scales smaller than a model grid box. Though significant amounts of deep water form in the model's Southern Ocean, the model is forced to simulate this process on a much larger spatial scale than the real world, so it seems likely that the spatial structure of simulated deep water formation and convection differs significantly from the real ocean.

These model shortcomings notwithstanding, it is difficult to escape the conclusion that the SAM is a major source of large-scale variability in the actual Southern Ocean. Since the main mode of variability in the real SH atmosphere is the annular mode, as it is in the model, the main mode of wind-stress forcing of the actual Southern Ocean has to be fluctuations of the surface westerlies. The details of the real ocean's response to this forcing have yet to be revealed; but the ocean model's response—Ekman drift at all longitudes—is exactly the first order response one would expect. The rest of the impacts (upwelling around Antarctica, downwelling further

north, increases in the strength of the circumpolar current, etc.) are similarly consistent with known and widely accepted principles of SH ocean dynamics. These mechanisms are unlikely to be significantly affected by the model shortcomings identified above.

We have demonstrated that SH geography facilitates an in-phase, zonally-symmetric oceanic response to a zonally-symmetric mode of atmospheric variability. Viewing the SH atmosphere and ocean as a synchonously-varying, zonally-symmetric system from the top of the atmosphere down to the ocean bottom constitutes a significant step towards understanding what controls internal variability in the SH. How might this idea fit in with previous ideas about SH climate variability? Two main ideas have been proposed previously: First, a series of papers have been published documenting the existence in the observations of an Antarctic circumpolar wave. This wave is characterized by eastward-propagating anomalies in surface pressure, temperature, wind, and sea-ice extent on time scales of 4-5 years (White and Peterson (1996) and White et al. (1998)). Second, Yuan and Martinson (2000) show statistical relationships between the ENSO phenomenon and Antarctic sea ice extent, implying that perhaps ENSO forces variability in this region. Of course, the Antarctic circumpolar wave and the links between Antarctic sea ice and ENSO may be robust. However, given the overwhelming dominance of the annular mode of the real atmosphere's internal variability on all time scales longer than a few days and the favorable geometry of the SH ocean, it seems likely that when adequate observations of all ocean variability in this region exist, most of the the variability will ultimately be traced not to the Antarctic circumpolar wave or ENSO but to the SAM.

The tendency towards co-variability of the atmosphere and ocean in this part of the world is even more significant in light of the accumulating evidence that the atmosphere responds to external forcing in patterns that resemble the SAM. For example, Fyfe et al. (1999) and Kushner et al. (2001) provide modeling evidence that the response of the SH atmosphere to anthropogenic

forcing projects strongly onto the SAM. Thompson and Solomon (2002) attribute recent trends in sea level pressure that resemble the SAM pattern to changes in stratospheric chemistry. And finally, Hall et al. (2002) demonstrate that the SAM-like patterns in surface pressure are preferentially excited by Milankovitch forcing. Thus from interannual to multi-millennial time scales, the SH atmosphere tends to respond to external forcing in a way that looks like the SAM. If it is possible to understand the response of the SH atmosphere to external forcing in terms of the SAM, then perhaps our results provide a way to understand the response of the SH ocean to external forcing as well.

Finally, it is worth noting the significance of our results for ocean biogeochemistry. Upwelling of deep water around the coast of Antarctica and its subsequent movement to the north is the principal means of nutrient supply for organisms living in the surface waters of the circumpolar ocean. This upwelling also results in significant outgassing of CO_2 to the atmosphere when dissolved CO_2 stored in the deep ocean water comes in contact with the atmosphere. Any changes in the strength of upwelling and the divergence of ocean water from the Antarctic continent such as those excited by SAM forcing would therefore be expected to alter the supply of nutrients to the circumpolar ocean and the rate at which the Southern Ocean releases CO_2 to the atmosphere. The fluctuations of the SAM, whether internally-generated or externally-forced, may have direct implications not only for marine life in the Southern Ocean, but also for the regulation of global atmospheric CO_2 levels.

Acknowledgments.

The authors wish to thank Ron Stouffer of the Geophysical Fluid Dynamics Laboratory for providing access to the model data, as well as John Fyfe and an anonymous reviewer for constructive criticism of the manuscript. The observed sea ice edge data shown in fig 10a were

derived from SMMR/SSMI ice concentration data provided by the National Snow Ice Data Center, University of Colorado, Boulder. This work is supported by NSF Grant ATM 00-02833. Alex Hall was also partly supported by a Lamont-Doherty Postdoctoral Fellowship while this work was carried out. This is Lamont-Doherty Earth Observatory contribution number XXXX.

References

Baker D.J., 1982: A note on the Sverdrup balance in the Southern Ocean. *J. Mar. Res.*, **40**, 21-26.

Broccoli A.J., S. Manabe, 1992: The effects of orography on midlatitude northern hemisphere dry climates. *J. Clim.*, **5**, 1181-1201.

Bryan K., 1969: Climate and the ocean circulation: III. The ocean model. *Mon. Wea. Rev.*, **97**, 806-827.

Bryan K., L. Lewis, 1979: A water mass model of the world ocean. *J. Geophys. Res.*, **84(C5)**, 2503-2517.

DeWeaver E., S. Nigam, 2000a: Do stationary waves drive the zonal-mean jet anomalies of the northern winter? *J. Clim.*, **13**, 2160-2176.

DeWeaver E., S. Nigam, 2000b: Zonal-eddy dynamics of the North Atlantic Oscillation. *J. Clim.*, **13**, 3893-3914.

Fyfe J.C., G.J. Boer, and G.M. Flato, 1999: The Arctic and Antarctic Oscillations and their Projected Changes Under Global Warming. *Geophys. Res. Lett.*, **26(11)**, 1601-1604.

Gill A.E., K. Bryan, 1971: Effects of geometry on the circulation of a three-dimensional southern hemisphere ocean model. *Deep Sea Res.*, **18**, 685-721.

Gordon C.T., W. Stern, 1982: A description of the GFDL Global Spectral Model. *Mon. Wea. Rev.*, **110**, 625-644.

Hartmann D.L., F. Lo, 1998: Wave-driven zonal flow vacillation in the southern hemisphere. *J. Atmos. Sci.*, **55**, 1303-1315.

Hall A., A. Clement, A. Broccoli, and C. Jackson, 2002: Milankovitch forcing of annular modes. manuscript in preparation.

James I.N., P.M. James, 1992: Spatial structure of ultra-low frequency variability of the flow in a simple atmospheric circulation model. *Quart. J. Roy. Meteor. Soc.*, **118**, 1211-1233.

Kushner P., I. Held, T. Delworth, 2001: Southern hemisphere atmospheric circulation response to global warming. *J. Clim.*, in press.

Kwok R., 2000: Recent changes in Arctic Ocean se ice motion associated with the North Atlantic Oscillation. *Geophys. Res. Lett.*, **27**: 775-778.

Kwok R, D.A. Rothrock, 1999: Variability of Fram Strait ice flux and North Atlantic Oscillation. *J. Geophys. Res.*, **104(C3)**: 5177-5189.

Lee S., S. Feldstein, 1996: Mechanisms of zonal index evolution in a two-layer model. *J. Atmos. Sci.*, **53**, 2232-2246.

Limpasuvan V., D.L. Hartmann, 1999: Eddies and the annular modes of climate variability. *Geophys. Res. Lett.*, **26**, 3133-3136.

Limpasuvan V., D.L. Hartmann, 2000: Wave-maintained annular modes of climate variability. *J. Clim.*, **13**, 4414-4429.

MacDonald A.M., C. Wunsch, 1996: An estimate of global ocean circulation and heat fluxes. *Nature*, **382**, 436-439.

Manabe S., D.G. Hahn, 1981: Simulation of Atmospheric Variability. *Mon. Wea. Rev.*, **109**, 2260-2286.

Manabe S., R.J. Stouffer, M. Spelman, and K. Bryan, 1991: Transient responses of a coupled ocean-atmosphere model to gradual changes of atmospheric CO_2. Part I: annual-mean response. *J. Clim.*, **4**, 785-817.

Marotzke J., P. Stone, 1995: Atmospheric transports, the thermohaline circulation, and flux adjustments in a simple coupled model. *J. Phys. Oceanogr.*, **25**, 1350-1364.

Robinson W.A., 1996: Does eddy feedback sustain variability in the zonal index? *J. Atmos. Sci.*, **53**, 3556-3569.

Thompson D.W.J., J.M. Wallace, 2000: Annular modes in the extratropical circulation. Part I: Month-to-month variability. *J. Clim.*, **13**, 1000-1016.

Thompson D.W.J., S. Solomon, 2002: manuscript in preparation.

Toggweiler J.R., B. Samuels, 1995: Effect of Drake Passage on the global thermohaline circulation. *Deep Sea Res.*, **42**, 477-500.

White W.B., R.G. Peterson, 1996: An Antarctic circumpolar wave in surface pressure, wind, temperature, and sea ice extent. *Nature*, **380**, 699-702.

White W.B., S.C. Chen, and R.G. Peterson, 1998: The Antarctic circumpolar wave: a beta effect in ocean-atmosphere coupling over the Southern Ocean. *J. Phys. Ocean.*, **28**, 2345-2361.

Yu J.Y., D.L. Hartmann, 1993: Zonal flow vacillation and eddy forcing in a simple GCM of the atmosphere. *J. Atmos. Sci.*, **50**, 3244-3259.

Yuan X., D.G. Martinson, 2000: Antarctic sea ice extent variability and its global connectivity. *J. Clim.*, **13**, 1697-1717.

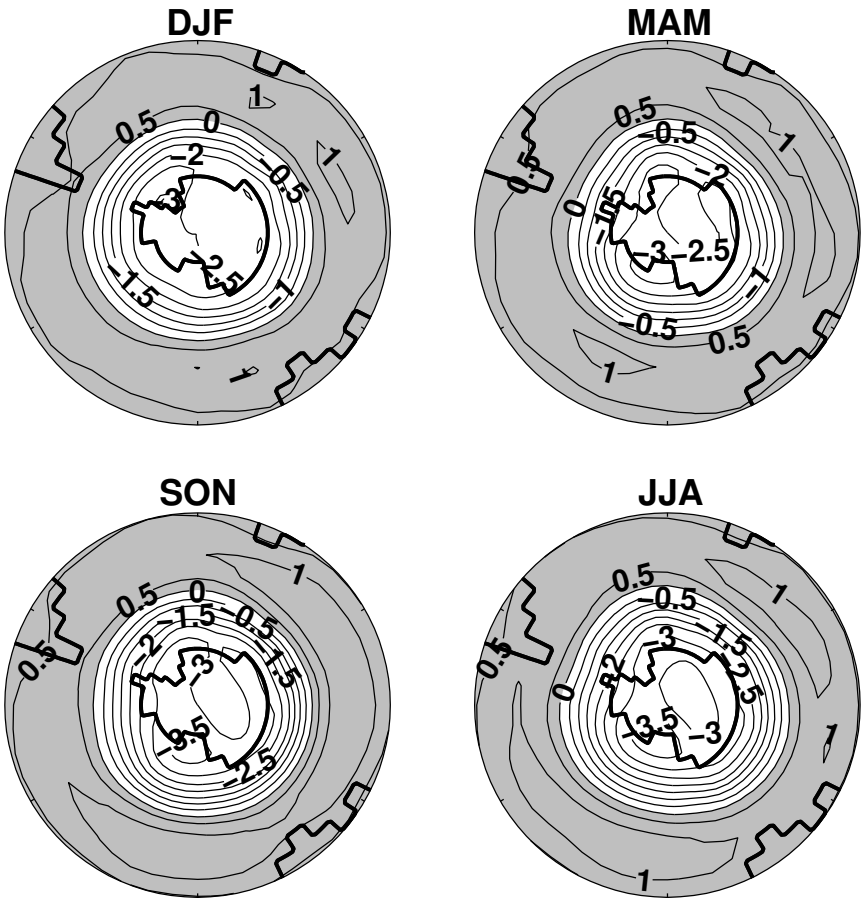

Figure 2: The patterns associated with the first EOFs of surface pressure (hPa) variability for all four seasons in the SH. All surface pressure data poleward of 9°S is included in the EOF computation. For DJF, MAM, JJA, and SON, the patterns shown account for 39%, 30%, 34%, and 24% of the variance, respectively. Note that fig 1b is identical to the panel marked JJA in this figure.

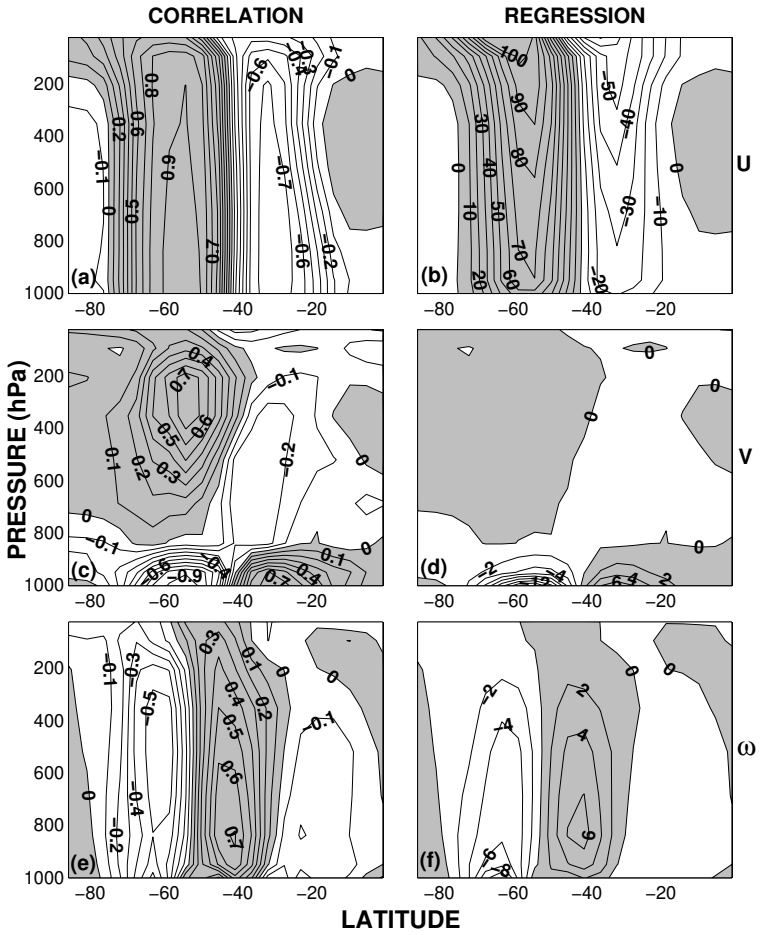

Figure 3: Correlation and regression coefficients between annual-mean, zonally-averaged zonal, meridional, and vertical winds throughout the atmosphere and the annual-mean SAM index. Since the SAM index is dimensionless with unit variance, units of the regression coefficients are the same as the units of the winds themselves: cm/s for U and V and 10^{-6} hPa/s for ω.

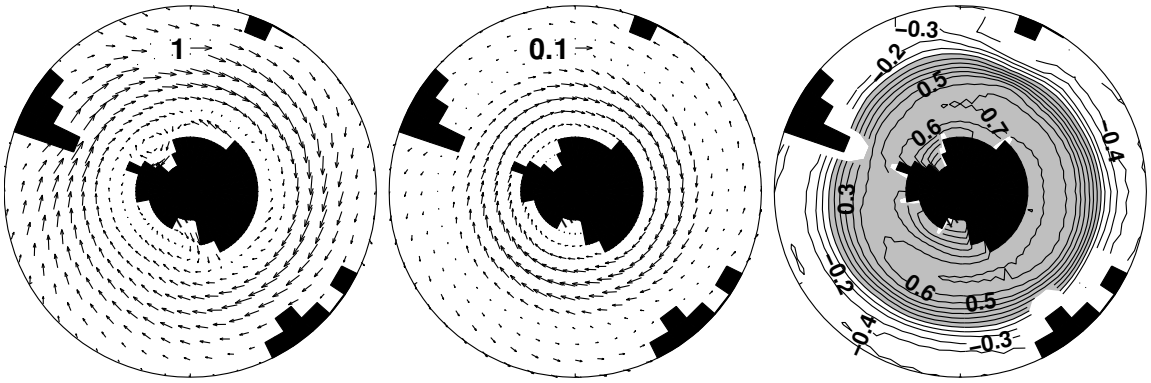

Figure 4: (a) the annual-mean climatological wind stress imposed on the ocean by the model atmosphere in the circumpolar region. (b) the regression of annual-mean wind stress onto the annual-mean SAM index. Regressions for the zonal and meridional components of the wind-stress were calculated separately. Units for (a) and (b) are dynes/cm^2. For clarity, every other arrow in each latitude row is suppressed in these two panels. Arrows illustrating the scaling of the vectors are shown in the top middle of the panels. (c) the correlation between the zonal component of the annual-mean wind stress and the annual-mean SAM index.

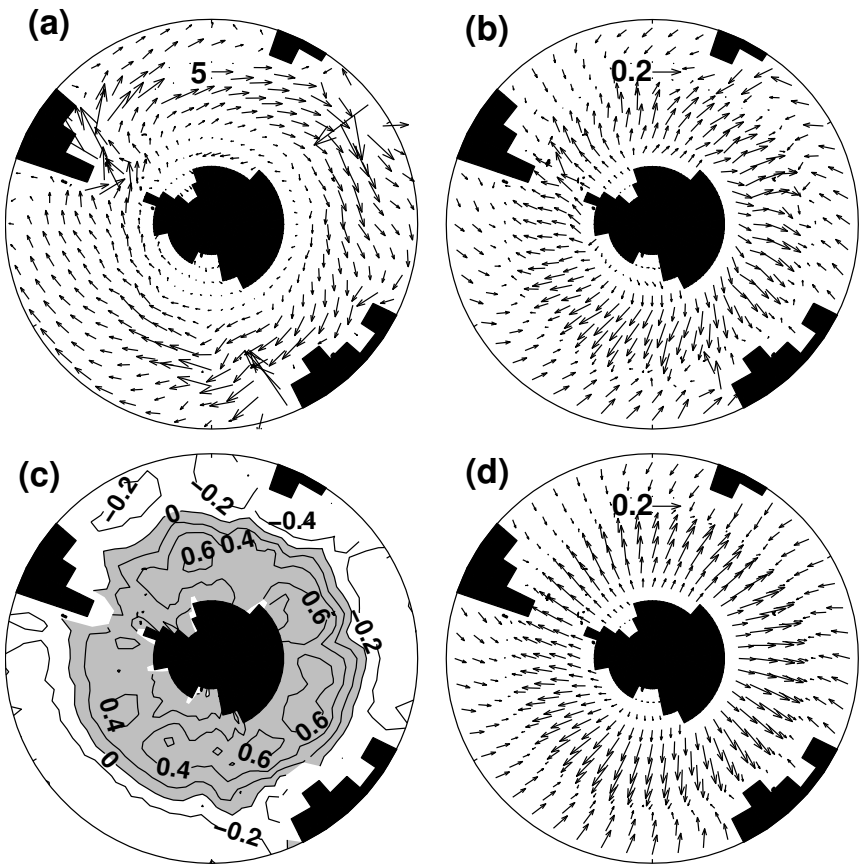

Figure 5: (a) the annual-mean climatological surface currents simulated by the ocean model. (b) the regression of annual-mean surface currents onto the annual-mean SAM index. Regressions for the zonal and meridional components of the surface currents were calculated separately. (c) the correlation between the meridional component of the annual-mean surface current and the annual-mean SAM index. (d) The Ekman drift that would result if the wind-stress pattern shown in fig 4b were imposed on the surface layer of the ocean model. Units for (a), (b), and (d) are cm/s. For clarity, every other arrow in each latitude row is suppressed. Arrows illustrating the scaling of the vectors are shown in the top middle of these three panels.

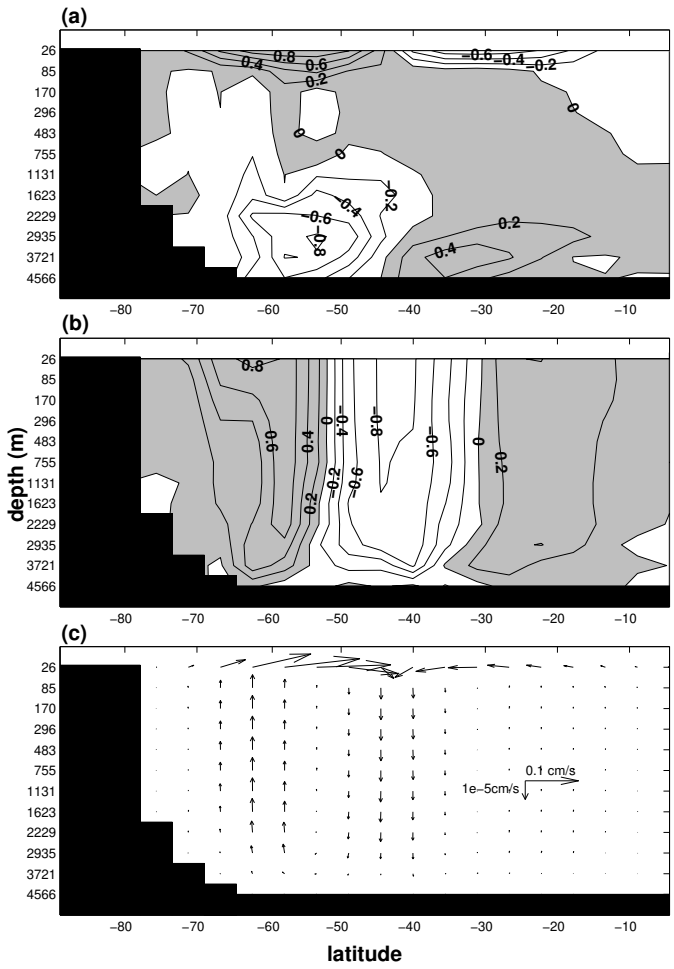

Figure 6: (a) the correlation between zonal-mean, annual-mean meridional currents throughout the SH ocean and the annual-mean SAM index. (b) the correlation between zonal-mean, annual-mean vertical currents throughout the SH ocean and the annual-mean SAM index. (c) the regressions of zonal-mean, annual mean meridional and vertical currents onto the annual-mean SAM index. Arrows illustrating the scaling of the two components of the vectors are shown in at the right. All latitudes and depths with some ocean grid points are depicted as ocean. The topography shown therefore does not accurately capture the complexity of the model's bottom topography.

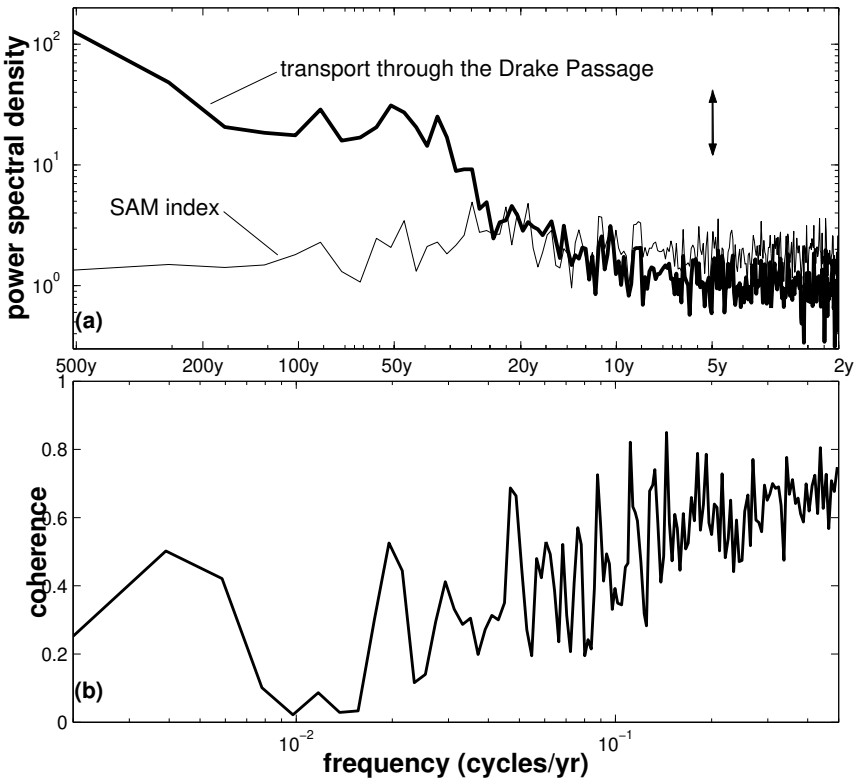

Figure 7: (a) spectra of both the circumpolar current, as measured by the annual-mean transport through the Drake Passage, and the annual-mean SAM index. The confidence interval for both spectra is the same, and is shown by the double-headed arrow in the upper right side of the plot. (b) the coherence between the strength of the circumpolar current and the SAM index. Varying between 0 and 1 and analogous to the correlation coefficient, coherence measures the relationship between two time series as a function of time scale. Time scales in years are displayed in between the two panels.

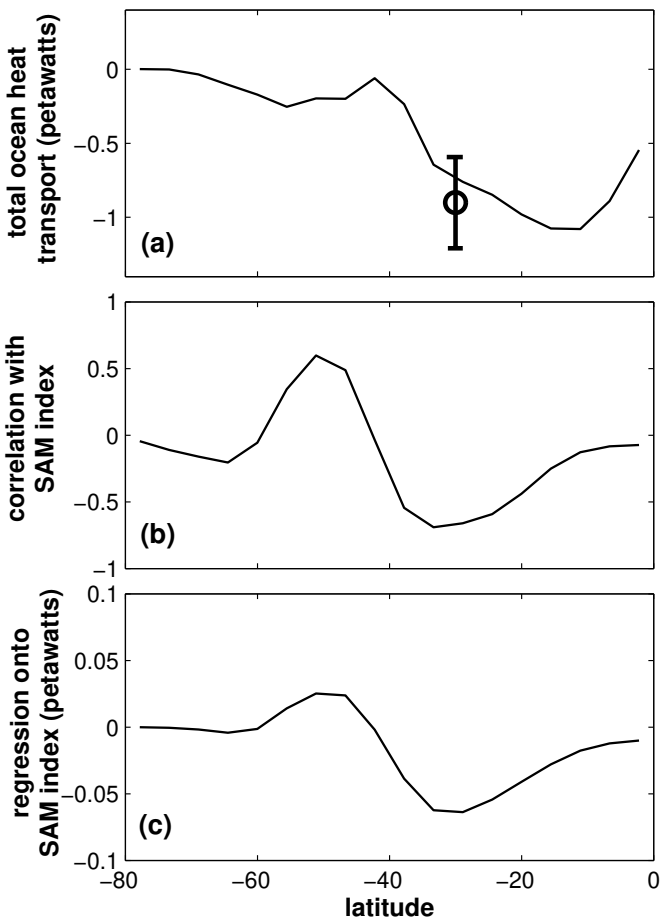

Figure 8: (a) the annual-mean, zonal-mean simulated ocean heat transport in the SH. Southward heat transport has a negative sign. Also shown, with a circle and associated error bars, is estimated observed ocean heat transport across 30°S from MacDonald and Wunsch (1996). (b) the correlation of the annual-mean, zonal-mean ocean heat transport with the annual-mean SAM index. (c) as in (b), except regression coefficients are shown.

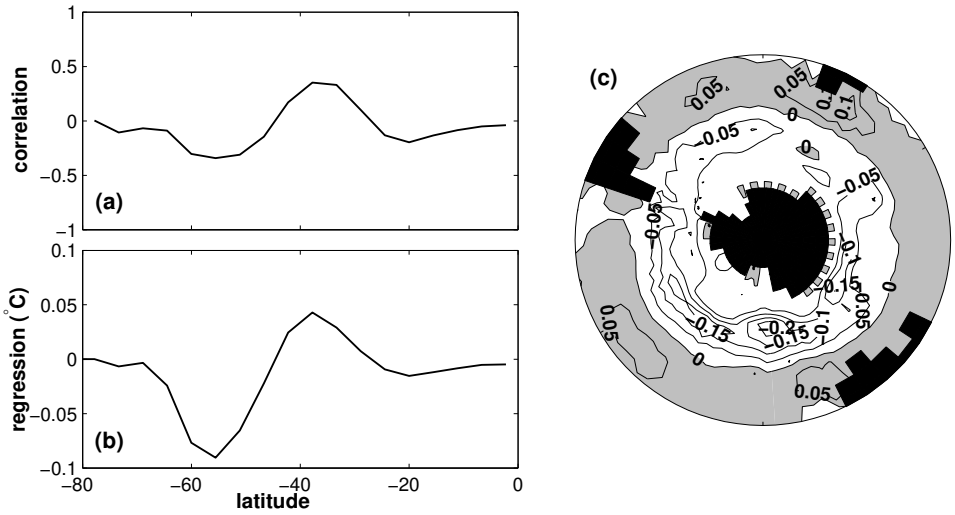

Figure 9: (a) correlation between zonal-mean, annual-mean SST and the annual-mean SAM index throughout the SH. (b) as in (a), except regression coefficients are shown. (c) the regression of annual-mean SST onto the annual-mean SAM index throughout the circumpolar region.

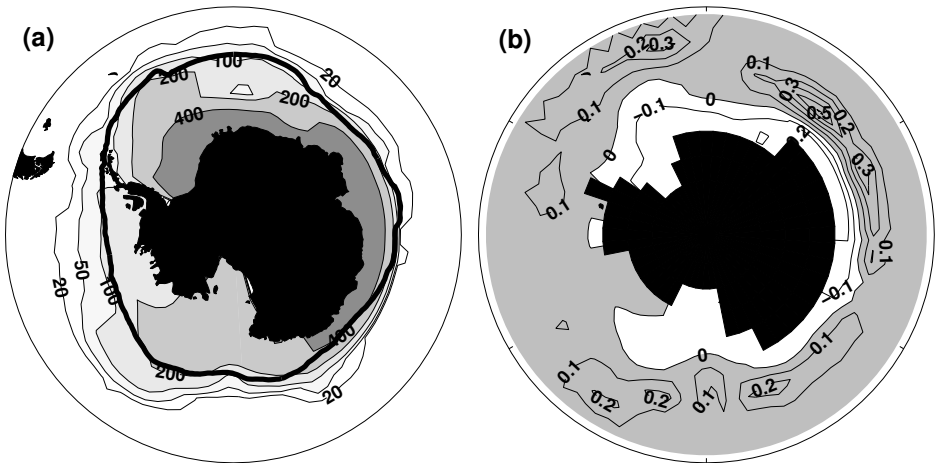

Figure 10: (a) climatological mean simulated and observed sea ice averaged from June through November (JJASON). The simulated sea ice field is quantified in terms of sea ice thickness (cm) and is shown with thin black contours and grey shading. The observed sea ice field is quantified in terms of ice concentration. The contour corresponding to 30% ice concentration is shown with a thick line. Observed ice concentrations were obtained from Yuan and Martinson (2000). Because of the difference between model and observation in the way sea ice amount is quantified, it is impossible to make a definitive comparison between the two. Still, this panel shows that the model has sea ice in approximately the same locations as the observations with approximately the same areal coverage of sea ice. (b) the correlation between JJASON simulated sea ice thickness and the JJASON SAM index.

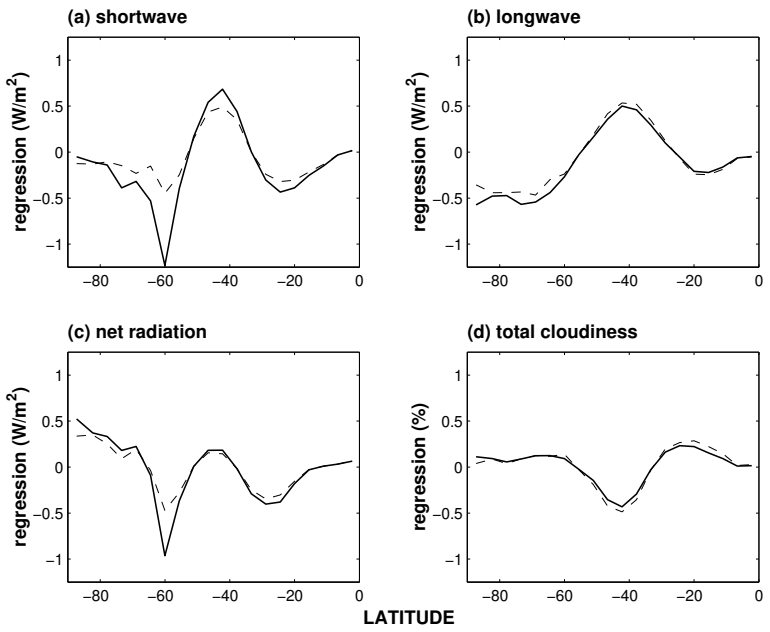

Figure 11: The regression of annual-mean, zonal-mean atmospheric quantities onto the annual-mean SAM index (solid lines). Correlation coefficients between the two time series are also shown as dashed lines. (a) net incoming shortwave radiation at the top of the atmosphere. (b) net outgoing longwave radiation at the top of the atmosphere. (c) net incoming radiation (shortwave - longwave) at the top of the atmosphere. (d) total cloudiness, measured by the percent of time the sky is covered by cloud.

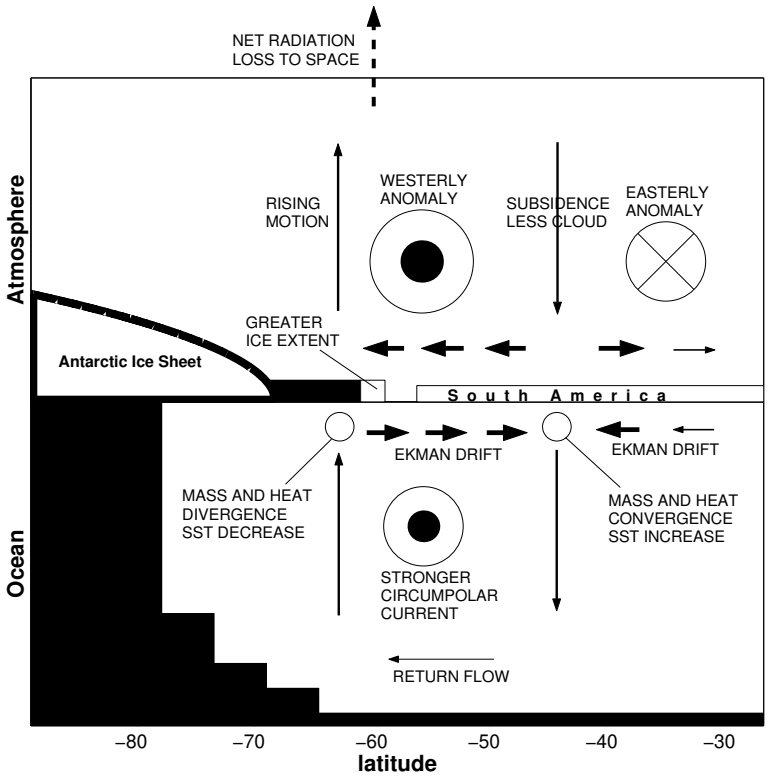

Figure 12: Schematic drawing of the changes in the atmosphere and ocean that occur when the SAM index is positive.

quantity	mean value	positive SAM	correlation
(a) sfc zonal winds (55.6°S)	3.87 m/s	0.85 m/s	0.95
(b) sfc meridional winds (55.6°S)	-0.94 m/s	-0.24 m/s	-0.94
(c) sfc zonal winds (33.3°S)	1.40 m/s	-0.31 m/s	-0.76
(d) sfc meridional winds (33.3°S)	-0.31 m/s	0.11 m/s	0.75
(e) vertical motion (64.5°S)	-75.4 X 10^{-6} hPa/s	-8.4 X 10^{-6} hPa/s	-0.50
(f) vertical motion (42.2°S)	-13.7 X 10^{-6} hPa/s	10.2 X 10^{-6} hPa/s	0.71
(g) net radiation (ice edge, 60.0°S)	-61.9 W/m^2	-1.4 W/m^2	-0.47
(h) meridional sfc flow (60.0°S)	0.68 cm/s	0.21 cm/s	0.96
(i) meridional sfc flow (33.3°S)	0.127 cm/s	-0.081 cm/s	-0.76
(j) vertical motion (sfc, 62.2°S)	27.7 X 10^{-6} cm/s	11.5 X 10^{-6} cm/s	0.86
(k) vertical motion (sfc, 44.5°S)	74.4 X 10^{-6} cm/s	-9.7 X 10^{-6} cm/s	-0.84
(l) SH ice coverage	167.4 X 10^5 km^2	8.9 X 10^5 km^2	0.51
(m) transport through Drake Passage	76.1 Sv	0.95 Sv	0.49
(n) heat transport (51.1°S)	-0.198 PW	0.038 PW	0.60
(o) heat transport (33.3°S)	-0.644 PW	-0.094 PW	-0.69
(p) SST (55.6°S)	1.84°C	-0.14°C	-0.34
(q) SST (37.8°S)	14.3°C	0.063°C	0.35

Table 1: First column: the zonal-mean values of the climatic variables shown in fig 12. Second column: the anomaly in those variables typically associated with a 1.5 standard deviation positive anomaly in the SAM index. The magnitude of the SAM index exceeds 1.5 standard deviations approximately once every seven years. Third column: the correlation between those variables and the SAM index. The horizontal double line separates climatic variables associated with the atmosphere and ocean.